J. COMBIN. MATH. COMBIN. COMPUT. 127b (2025) 6867--6884

Journal of Combinatorial Mathematics and Combinatorial Computing
www.combinatorialpress.com/jcmcc

Combinatorial Press

A study on the integrated application of computational methods in low-voltage distributed photovoltaic user regulation and station side-end autonomy strategies

Guocheng Li[1], Cong Wang[1], Zeguang Lu[1], Ze Zhang[1,✉], Xiaoran Li[1], Xiaoqin Wang[2]

[1] *State Grid Dezhou Power Supply Company, Dezhou, Shandong, 253000, China*

[2] *Sichuan Changduo Electric Power Engineering Co., Ltd., Zibo, Shandong, 255000, China*

ABSTRACT

This paper follows the active reactive power cooperative control strategy of station voltage autonomy, combines the operation scenarios of the autonomous control strategy within the group, and establishes the reactive power optimization objective function of the low-voltage distribution network to improve the voltage quality and reduce the active loss, which takes into account the installation location of reactive power compensation device, and the constraints include the system power balance constraints and voltage quality constraints. In order to solve the reactive power optimization model of low-voltage distribution network containing distributed photovoltaic, the uniformity of the population distribution of the MPA algorithm is initialized using Bernoulli mapping, the inertia weight function and elite strategy of nonlinear attenuation are introduced to enhance the optimization capability of the MPA algorithm in the iterative process, and the eddy-current and fish aggregation effects are applied to widen the scope of optimization search. The network loss and voltage amplitude of the proposed strategy are analyzed to compare the changes of node voltage, voltage offset, objective function value and branch circuit active loss before and after the voltage autonomous reactive power control of low voltage stations. After adopting the optimization strategy of voltage autonomous reactive power control for LV stations, the branch circuit active loss of LV distribution network decreases with the increase of the proportion of distributed PV, and the branch circuit active loss of LV distribution network can be reduced by up to 60%.

Keywords: distributed PV, distribution network reactive power optimization, reactive power compensation, MPA algorithm

1. Introduction

Energy is related to the lifeblood of national economic development, and the problems of energy scarcity and environmental pollution cannot be ignored. According to the estimation of the International Energy Agency, global energy consumption will increase by at least 25% by 2040. In recent years, due to the gradual scarcity of fossil energy, all countries have paid great attention to

✉ Corresponding author.
E-mail address: zhangzedq0801@163.com (Z. Zhang).
Received 20 February 2024; Revised 25 April 2024; Accepted 20 November 2024; Published Online 16 April 2025.
DOI: 10.61091/jcmcc127b-375

renewable energy, and solar photovoltaic has been rising in the proportion of energy composition due to its advantages of low-cost, non-pollution, wide distribution, and relatively simple development [1-4]. Compared to other renewable energy sources such as wind power, distributed PV is able to be applied on a large scale in these areas because it does not require large tracts of land, and relatively expensive land can be utilized, which makes distributed PV an ideal choice for clean energy generation in urban and other densely populated areas [5-8]. Overall, the widespread use of distributed PV power can effectively solve the environmental pollution problems caused by fossil fuels, short construction time, and can be developed simultaneously with other industries, which is one of the high-quality new energy sources to replace fossil fuels.

Photovoltaic in the scale of utilization of the main form is divided into centralized and distributed two kinds, compared with the centralized, distributed photovoltaic power generation energy utilization is higher, the economy is better, and the user can generate electricity for self-consumption, so in recent years the amount of photovoltaic grid-connected continues to rise [9-11]. According to the CEC data, in 2022, China's PV cumulative installed capacity of 392.61 million kilowatts, of which the cumulative installed capacity of distributed PV more than 15,000 million kilowatts, accounting for about 40% of the total installed capacity, distributed PV in the low-voltage distribution stations is a straight line rise. However, due to the PV processing and load can not be normally matched, in the sunny warm environment of the station area voltage overrun risk increases, and single-phase photovoltaic access to the stochastic characteristics, resulting in an increase in transformer loads, transmission line losses increase, thus reducing the service life of the distribution network equipment [12-15]. Based on this, it is difficult to cope with the above problems with the traditional distribution network control methods, and explore the new low-voltage distributed PV user regulation and station area side-end autonomy strategies to provide theoretical support for the energy industry.

This paper summarizes the principles and output characteristics of distributed photovoltaic power generation, sets the objective function of intra-group autonomous control in order to achieve the node voltage not to exceed the limit and the network loss minimization, and outlines the operation scenarios of intra-group autonomy in each case. From the problem of station voltage overrun, the optimization model of low voltage station voltage autonomous reactive power control is proposed, the system power balance constraints and voltage quality constraints are set, and the improved MPA algorithm is applied to obtain the installation location of reactive power compensation devices. Analyze the performance of Dist-S strategy and other benchmark method strategies in this paper, and compare the network loss and three-phase voltage distribution of each method strategy by scenario. Compare the changes in objective function values and branch circuit active losses before and after control of Dist-S strategy.

2. Principles and output characteristics of distributed photovoltaic power generation

2.1. Basic Principles of Photovoltaic Power Generation

Photovoltaic cells convert light energy into electrical energy through photoelectric or chemical reactions. When a photovoltaic cell that is illuminated by light is connected to a circuit element, a photocurrent occurs in the circuit element, and a corresponding voltage is generated at both ends of the circuit element at the same time. The equivalent circuit of a photovoltaic cell is shown in Figure 1.

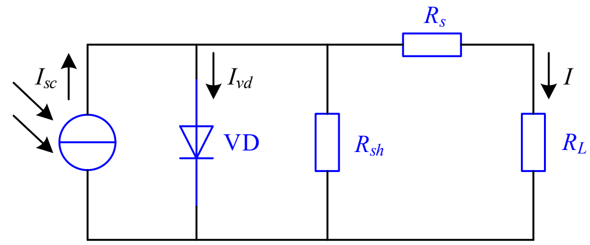

Fig. 1. Equivalent circuit of photovoltaic cells

where R_{sh} represents the equivalent parallel resistance. R_s represents the equivalent series resistance, R_L is the equivalent load resistance. Generally R_s is small and R_{sh} is large. It can be obtained from Fig. 1:

$$I = I_{sc} - I_{sh} - I_{vd} \tag{1}$$

where I is the output current of the PV module, I_{sc} is the photogenerated current. I_{sh} is the leakage current of the PV module, and I_{vd} is the reverse saturation current of the PV cell, which denotes the total diffusion current through the PN, and its direction is opposite to I_{sc}:

$$I_{vd} = I_{d0}\left(e^{qe/AkT} - 1\right) \tag{2}$$

where q is the charge of the electron, $1.6\times10^{-19}\,\mathrm{C}$. k is the Boltzmann constant, $1.38\times10^{-23}\,\mathrm{J/K}$. A is a constant factor ($A=1$ when the positive bias voltage is large, $A=2$ when the positive bias voltage is small). I_{d0} is the saturation current of the PV cell without light. Where the saturation current of the PV cell without light is:

$$I_{d0} = AqN_C N_V \left[\frac{1}{N_A}\left(\frac{D_n}{\tau_n}\right)^{1/2} + \frac{1}{N_D}\left(\frac{D_p}{\tau_p}\right)^{1/2} \right] e^{-\frac{Eg}{KT}} \tag{3}$$

where $N_C N_V$ is the effective density of states in the conduction and valence bands. $N_A N_D$ is the concentration of the host and donor impurities. $D_n D_q$ is the diffusion coefficient of electrons and holes. $\tau_n \tau_p$ is the oligon lifetime of the electron and hole. E_g is the band gap of the semiconductor material.

The calculation of the load current I is carried out using equation (1):

$$I = I_{sc} - I_{d0}\left(e^{\frac{q(U_L + I_L R_s)}{AkT}} - 1\right) - \frac{U_L + I_L R_s}{R_{sh}} \tag{4}$$

An ideal PV cell is usually negligible due to the fact that R_s is in series and very small, and R_{sh} is in parallel and very large, both of which are intrinsic resistances of the PV cell itself. A perfect PN junction characteristic equation is finally derived:

$$I = I_{sc} - I_{d0}\left(e^{\frac{qU_L}{AkT}} - 1\right) \tag{5}$$

The voltage across the load can be calculated from equation (5) as:

$$U_L = \frac{AkT}{q}\ln\left(\frac{I_{sc} - I}{I_{d0}} + 1\right) \tag{6}$$

2.2. Output Characteristics of Distributed Photovoltaic Power Generation

The electricity formed by PV power generation cannot normally be used directly and needs to be processed and optimized in several ways. Typical distributed PV power generation system components are PV arrays, converters, inverters, controllers and so on. Among them, the PV array is responsible for energy conversion, converting solar energy into DC electricity. The converter boosts and choppers the DC power, and the DC power can be directly supplied to the DC load. In addition, the controller tracks the changes in voltage and frequency of the external grid in real time and outputs pulse width modulated waveforms to control the inverter. The inverter inverts the DC power into AC power for grid connection or for supplying AC loads. For some distributed photovoltaic power generation, battery packs can also be configured to store the power [16-17].

In order to study the impact of distributed PV power generation systems on the distribution network, the study of the output characteristics of PV modules is necessary. The equivalent circuit diagram of the PV module is shown in Fig. 2, in the ideal PV module, the series and shunt resistors are excluded, but in practice, due to the presence of the resistance coefficients of the PV semiconductor and the non-ideal PN junction diode, the equivalent circuit of the PV module contains the series and shunt resistors.

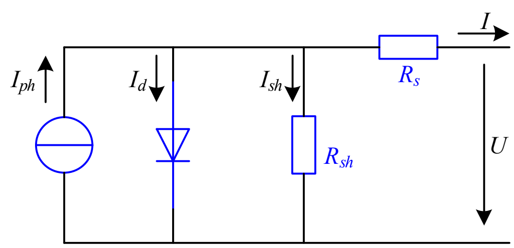

Fig. 2. The equivalent circuit diagram of photovoltaic components

According to the circuit diagram shown in Fig. 2, the characteristic equations of the photovoltaic cell circuit I and voltage U can be obtained as:

$$I = I_{pk} - I_{sat}\left\{\exp\left[\frac{q\left(U + IR_s\right)}{AkT} - 1\right] - \frac{U - IR_s}{R_{sh}}\right. \tag{7}$$

where I_{sat} is the saturation current of the diode. k is the Bormann's constant, q is the number of charges, and T is the temperature of the PV cell circuit under standard test conditions. Based on the above analysis, the output characteristics of the PV cell can be obtained.

3. Optimization of voltage-autonomous reactive power control for low-voltage stations with distributed photovoltaics

3.1. Intra-cluster Autonomous Control Strategy

Containing high penetration rate low voltage distributed PV distribution station area following the principle of regional autonomy, the introduction of intelligent fusion terminal equipment integrating the functions of power supply and consumption information collection in the distribution station area, data collection from each collection terminal or power meter, cooperative calculation, localized analysis and decision-making, equipment status monitoring and communication networking, etc. is installed in the distribution station area.

Using the edge computing function of the convergence terminal, it realizes local cooperative control of distributed PV clusters, dynamically optimizes the voltage quality of the station area, and adjusts the reverse load rate of the distribution transformer. Aiming at the problem of voltage overrun in the station area, following the basic principle of "reactive power first, active power later, and global cooperative control in the station area", this paper proposes the reactive power control autonomy strategy.

The autonomy within the cluster is achieved by the cluster control platform by controlling the active and reactive power output of the PV power station within the cluster and the reactive power compensation device output to realize that the node voltage does not exceed the limit and the network loss is minimized, i.e., the model contains two objective functions:

$$\min f_3 = \sum_{n=1}^{N} \left| U_n - U_0 \right| \tag{8}$$

$$\min f_4 = \frac{1}{2} \sum_{n=1}^{N} \sum_{l} i_{nl}^2 r_{nl} \tag{9}$$

Where N denotes the total number of nodes in the cluster. U_n denotes the voltage amplitude of node n in the cluster, and U_n is also expressed as a scalar value. l denotes the set of branches connected to node n starting at node n and ending at l. i_{nl} denotes the branch current and r_{nl} denotes the branch resistance.

The distribution network current constraints under the intra-cluster autonomy strategy are the same as the current constraints in the inter-cluster coordination constraints, which are different from the power constraints of each PV plant in the cluster, the safe operation constraints of each node voltage and each branch current in the cluster, and the reactive power compensation device output constraints.

1) PV power constraints

$$0 \le P_{PV,n} \le P_{PV,n}^{\max} \tag{10}$$

$$P_{PV,n}^2 + Q_{PV,n}^2 \le S_{PV,n}^2 \tag{11}$$

$$-P_{PV,n}^2 \frac{\sqrt{1-\cos\theta^2}}{\cos\theta} \le Q_{PV,n} \le P_{PV,n}^2 \frac{\sqrt{1-\cos\theta^2}}{\cos\theta} \tag{12}$$

$$0 \le P_{PV,n} \le P_{PV,n}^{\max} \tag{13}$$

$$P_{PV,n}^2 + Q_{PV,n}^2 \le S_{PV,n}^2 \tag{14}$$

where $P_{PV,n}^{\max}$ denotes the maximum active output of the n th PV plant and $\cos\theta$ denotes the minimum power factor of the PV plant.

2) Safe operation constraints

$$U_n^{\min} \le U_n \le U_n^{\max} \tag{15}$$

$$0 \le i_{ij} \le i_{ij}^{\max} \tag{16}$$

Where $U_n^{\min}$ and $U_n^{\max}$ denote the upper and lower limits of the node voltages within the cluster, respectively, which are the same as the upper and lower limits of the dominant node voltages, and the same as the constraints on the safe operation during the inter-cluster coordinated control, which is taken as the range of safe operation for the node voltages within the cluster from 0.95 p.u. to 1.05 p.u. The $i_{ij}^{\max}$ denotes the branch $i-j$ maximum current limit.

3) Reactive power compensation device operation constraints

$$Q_{SVC,n}^{\min} \le Q_{SVC,n} \le Q_{SVC,n}^{\max} \tag{17}$$

Where $Q_{SVC,n}$ denotes the n th reactive power output of the reactive compensation device in the cluster. $Q_{SVC,n}^{\max}$ and $Q_{SVC,n}^{\min}$ denote the upper and lower limits of the reactive power output of the reactive compensation device, respectively.

According to the node voltage operation status within the cluster and whether the node voltage can be operated in the safe range only by regulating the reactive power output of the PV plant, the intra-cluster autonomy can be roughly categorized into the following operation scenarios:

1) Node voltage operation within the safe range. In this scenario, by regulating the reactive power output of distributed PV power plants in the cluster, the node voltage is within the safe range while minimizing the cluster network loss.

2) The node voltage mildly exceeds the upper limit, and only by adjusting the reactive power output of distributed PV power plants in the cluster, the node voltages in the cluster can be restored to the safe range, so as to realize the safe operation within the cluster.

3) The node voltage seriously exceeds the upper limit, and the safe operation of the node voltage cannot be realized only by regulating the reactive power output of distributed PV power plants in the cluster. In this scenario, it is also necessary to reduce the active output of distributed PV power plants to restore the node voltages within the cluster to the safe range. In order to realize the maximum consumption of distributed PV as much as possible, this paper sets the maximum reduction of active output of each PV power plant by 2%.

4) The node voltage seriously crosses the lower limit, and the safe operation of the node voltage cannot be realized only by regulating the reactive power output of distributed PV power plants in the cluster. In this scenario, it is also necessary to regulate the reactive power output of the reactive power compensation device so that the node voltage in the cluster can be restored to a safe range.

3.2. Reactive power optimization model for LV distribution network with distributed PV

The reactive power optimization of a power system refers to the adjustment of the transformer taps as far as possible by ensuring the safe operation of the grid. Reasonable planning and casting reactive power compensation devices to realize the local balance of reactive power and reduce the delivery of reactive power on the line. This in turn achieves the purpose of improving the node voltage quality and reducing the network active loss.

For the configuration of reactive power compensation in low-voltage distribution networks, the main problems to be solved are where to install reactive power compensation devices, how large the capacity of reactive power compensation devices to be installed, and how to determine the switching gear of reactive power compensation devices. Therefore, the optimal allocation of reactive power in low-voltage distribution networks is essentially a nonlinear mixed-integer programming problem with discrete variables and multiple constraints.

3.2.1. Objective function. Improvement of voltage quality and reduction of active loss is the main purpose of reactive power optimization in LV distribution network, the total network loss of LV distribution station area is equal to the active power injected into the high voltage side of the distribution transformer of the station area minus the active power absorbed by all the load nodes in the station area, the expression is shown in equation (18):

$$\min f\left(U,\theta,Q_c\right)=P_s\left(U,\theta,Q_c\right)+\sum_{i=1}^{n_{pv}}P_{pv,i}\left(S,T\right)-\sum_{i=1}^{n_l}P_{l,i} \tag{18}$$

where P_s denotes the active power injected into the high voltage side of the distribution transformer. U and θ denote the magnitude and phase angle of the nodal voltage, state variables, respectively. Q_c denotes the compensation capacity of the capacitor (or reactor), decision variables. S , T denote the light intensity and temperature during the actual operation of the PV power supply, respectively. $P_{pv,i}$ denotes the active power output from the ith distributed PV power supply. n_{pv} denotes the total number of distributed PV power sources in the station area, and $P_{l,i}$ denotes the active power of the load at node i.

3.2.2. Basic constraints:

1) System power balance constraints. The equation constraints for the distributed PV nodes and their grid connection points are shown in the above equation, while the equation constraints for the other load nodes are shown in equation (19):

$$\begin{cases} \Delta P_i = P_{g,i} - P_{l,i} - U_i \sum_{j \in i} U_j (G_{ij} \cos\theta_{ij} + B_{ij} \sin\theta_{ij}) = 0 \\ \Delta Q_i = Q_{g,i} + Q_{c,i} - Q_{l,i} - U_i \sum_{j \in i} U_j (G_{ij} \sin\theta_{ij} - B_{ij} \cos\theta_{ij}) = 0 \end{cases} \tag{19}$$

where $P_{g,i}$, $Q_{g,i}$ are the active and reactive power injected by the source at node i. $P_{l,i}$, $Q_{l,i}$ are the active and reactive power of the loads at node i, and Q_{ci} is the reactive compensation capacity at node i, discrete variables.

2) Voltage quality constraint. According to the provisions of the national standard power quality supply voltage deviation, for the 220V single-phase power supply of low-voltage distribution network, the permissible deviation value of the user's receiving end voltage is $-10\% \sim +7\%$ of the rated voltage. In order to ensure the provision of qualified power to the users, the optimal configuration calculation of reactive power compensation should ensure that the deviation of all node voltages within the distribution area is within the qualified range during normal operation. The nodal voltage U is a state variable related to the reactive power compensation device casting amount Q_c, and the constraints of voltage quality are shown in Equation (20):

$$\underline{U}_i < U_i(Q_c) < \overline{U}_i \tag{20}$$

where $\underline{U}_i$ and $\overline{U}_i$ denote the lower and upper bounds of the node i voltage U_i, respectively.

3.2.3. Total number of compensating device installation constraints. In order to reduce the investment cost of reactive power compensation and improve the economy of stable operation of distribution networks, the number of installation points of reactive power compensation devices in distribution networks should not be too many. Different from the centralized reactive power compensation optimal allocation calculation, not only the limitation of the compensation capacity of each installation point, but also the limitation of the total number of installation points of reactive power compensation devices in the whole station area should be considered in the decentralized reactive power optimal allocation calculation, as shown in equations (21) and (22):

$$\underline{Q}_{c,i} < Q_{c,j} < \overline{Q}_{c,i} \tag{21}$$

$$0 \le \sum_{i=1}^{m} \operatorname{sgn}(Q_{c,i}) \le N_{sum} \tag{22}$$

where $Q_{c,t}$, $\overline{Q}_{c,i}$ are the lower and upper limits of the compensation capacity $Q_{c,t}$ of the i th reactive power compensation device, respectively. N_{sum} denotes the upper limit of the total number of reactive power compensation device installations allowed in the distribution area, and m denotes the total number of candidate installation nodes of reactive power compensation devices, and when the reactive power optimization model adopts the decentralized compensation method, all the load nodes in the station area can be selected as candidate installation nodes. The specific meaning of the symbolic function $\operatorname{sgn}(Q_{c,i})$ is shown in equation (23):

$$\operatorname{sgn}(Q_{c,t}) = \begin{cases} 1, Q_{c,i} > 0 \\ 0, Q_{c,t} = 0 \end{cases} \tag{23}$$

Obviously, when the compensation capacity of the candidate point is equal to zero, then the node does not need to install reactive power compensation device. When the compensation capacity of the candidate point is greater than zero, then the node needs to install reactive power compensation device. It can be seen that the above optimization model directly takes all load nodes as candidate installation nodes, and obtains the installation position of reactive power compensation device by solving the optimization model, which can avoid the subjectivity in the selection of the installation point of reactive power compensation device.

3.3. Improved marine predator optimization algorithm

Compared with other traditional algorithms such as genetic algorithm and particle swarm algorithm, the marine predator algorithm (MPA) algorithm is simple in parameter setting, and in the final stage of finding the optimal solution of the target, the predator not only wanders in the area where the preys gather more, but also through a certain period of time in order to reach the other areas where the preys are more dispersed, so that the predator can avoid being trapped in the local optimal solution, and its ability of global optimality search is stronger [18-19].

In order to further improve the performance of the algorithm, this paper proposes an improved marine predator algorithm (MO-MPA), which improves the initialization phase and iterative computation phase of the standard MPA algorithm, respectively.

3.3.1. Initialization based on Bernoulli mapping. The MPA algorithm first generates an initial model randomly in the search space, and the standard MPA algorithm population initialization formula is:

$$X_0 = X_{\min} + rand\left(X_{\max} - X_{\min}\right) \tag{24}$$

where X_0 is the initial solution. $X_{\min}$, $X_{\max}$ are the upper and lower bounds of the initial solution. $Rand$ is a vector of random numbers in the range 0-1.

In order to improve the uniformity of the distribution of the initial population distribution on the search space, this paper introduces the Bernoulli mapping into the initialization stage to improve the uniformity of the distribution of the initial population in the high-dimensional space, and the mapping formula is as follows:

$$Y_{u,v+1} = \begin{cases} Y_{u,v} / (1-\lambda), 0 < Y_{u,v} \le 1-\lambda \\ \left(Y_{u,v} - 1 + \lambda\right) / \lambda, 1-\lambda < Y_{u,v} < 1 \end{cases} \tag{25}$$

Where $u = 1, 2, \cdots, n$ is the number of individuals in the initial solution. $v = 1, 2, \cdots, m$ is the dimension of the solution. λ is the mapping constant. $Y_{u,v}$ is the location information of the u th individual in the vth dimension.

The population is initialized by Bernoulli mapping, and the standard MPA algorithm initialization formula is improved as:

$$X_0 = X_{\min} + \left(X_{\max} - X_{\min}\right) \times Y_{u,v} \tag{26}$$

An initial m-dimensional initial population X_0 is randomly obtained from Eq. (24), and the corresponding position information is calculated by Eq. (25), and then the position information is substituted into Eq. (26) to obtain the position information of the next dimensional solution vector, and keep looping the calculation to obtain the $n-1$ group of position information, which is substituted into Eq. (25) to obtain the n of all m-dimensional initial solutions. The initial population is defined as the prey matrix (Prey) and the optimal solution matrix is defined as the predator matrix (Elite), denoted as follows:

$$\Pr ey = \begin{bmatrix} X_{11} & X_{12} & \cdots & X_{1m} \\ X_{21} & X_{22} & \cdots & X_{2m} \\ \vdots & \vdots & \ddots & \vdots \\ X_{n1} & X_{n2} & \cdots & X_{nm} \end{bmatrix}_{n \times m} \tag{27}$$

$$Elite = \begin{bmatrix} X'_{11} & X'_{12} & \cdots & X'_{1m} \\ X'_{21} & X'_{22} & \cdots & X'_{2m} \\ \vdots & \vdots & \ddots & \vdots \\ X'_{n1} & X'_{n2} & \cdots & X'_{nm} \end{bmatrix}_{n\times m} \tag{28}$$

Where n is the population size. m is the number of variables in the reactive optimization model.

3.3.2. Introduction of nonlinear weights and elite strategies. After obtaining the initialized population, the population position needs to be adjusted to update the prey matrix and predator matrix, i.e., entering the iterative calculation stage of the MPA algorithm.

1) When the number of iterations is less than one-third of the maximum number of iterations, the step size updating formula and the prey matrix updating formula are respectively:

$$\begin{cases} S_i = R_B \otimes \left(Elite_i - R_B \otimes \Pr ey_i\right), i = 1, 2, \cdots, n \\ \Pr ey_i = \Pr ey_i + P \cdot R \otimes S_i \end{cases} \tag{29}$$

where R_B is the m-dimensional random vector generated using Brownian random walk. S_i is the move step matrix. R is the $R-m$-dimensional random number vector. P is a constant with value 0.5.

2) When the number of iterations is greater than one-third of the maximum number of iterations and less than two-thirds of the maximum number of iterations, the population needs to be divided into two parts for the update operation. The first half of the population step update formula and the prey matrix update formula are respectively:

$$\begin{cases} S_i = R_L \otimes \left(Elite_i - R_L \otimes \Pr ey_i\right), i = 1, 2, \cdots, n/2 \\ \Pr ey_i = \Pr ey_i + P \cdot R \otimes S_i \end{cases} \tag{30}$$

where R_L is the m-dimensional random vector generated using Brownian random walk.

The second half of the population step update formula and the prey matrix update formula are, respectively:

$$\begin{cases} S_i = R_B \otimes \left(Elite_i - R_B \otimes \Pr ey_i\right), i = n/2, \cdots, n \\ \Pr ey_i = Elite_i + P \cdot CF \otimes S_i \end{cases} \tag{31}$$

Where CF is the adaptive parameter of step size S_i, which is calculated as $CF = \left(1 - \frac{t}{T}\right)^{\left(\frac{2t}{T}\right)}$. t and T are the current iteration number and the maximum iteration number. Thus, the prey matrix update formula can be improved as:

$$Prey_i = Prey_i + W \cdot P \cdot R \otimes S_i \tag{32}$$

3) When the number of iterations is greater than two-thirds of the maximum number of iterations, an elite replacement strategy is introduced to avoid falling into a local optimum near the end of the iteration. The step size update formula and the prey matrix update formula are respectively:

$$\begin{cases} S_i = R_L \otimes \left(R_L \otimes Elite_i - \Pr ey_i\right), i = 1, 2, \cdots, n \\ \Pr ey_i = Elite_i + P \cdot CF \otimes S_i \end{cases} \tag{33}$$

Calculate the fitness value of the solution vectors at this point in time and apply the elite replacement mechanism to the solution vectors that are lagging behind in fitness with the following formula:

$$\Pr ey_{i,ineffective} = \Pr ey_{i,effective} \cdot R_{star} \cdot rand(-0.5, 0.5) / m \tag{34}$$

Where $Prey_{i,effective}$ is the 20% of individuals with the most backward adaptation. $Prey_{i,effective}$ is the 20% of individuals with the best adaptation. R_{star} is the Euclidean distance between the optimal individual and the individual closest to the optimal individual.

3.3.3. Jumping out of a local optimum process. To avoid the optimization process from falling into local optimum, the environmental effects of eddy currents and fish aggregation effects (FADs) are introduced, i.e., the predator wanders near the prey in 80% of the search space, and the remaining 20% wanders in different regions to achieve the global search, and are denoted as:

$$\Pr ey_l = \begin{cases} \Pr ey_i + CF\left[X_{\min} + R \otimes \left(X_{\max} - X_{\min}\right)\right] \otimes U, if\ r \le FADs \\ \Pr ey_i + \left[FADs(1-r) + r\right]\left(\Pr ey_{r1} - \Pr ey_{r1}\right), if\ r > FADs \end{cases} \tag{35}$$

Where r is a random number. $FADs$ value is a constant of 0.2. r_1, r_2 is the random subscript $\left(1 < r_1, r_2 < 2\right)$ of the prey matrix. The U is a m-dimensional binary vector.

3.3.4. Reactive power optimization process based on MO-MPA algorithm. For the above optimization model of voltage autonomous reactive power control for LV station area containing distributed PV, the MO-MPA algorithm is used to solve the problem, which mainly includes the following steps.

1) Input the original data of the station area, including the impedance of each line in the station area, the load of each node, and the rated capacity of each distributed PV power source. Initialize the population based on Bernoulli mapping, i.e., the initial value of distributed PV power output, and construct the prey matrix accordingly.

2) Calculate and compare the adaptation function values between the mean values of the first three optimal solutions and the optimal solution according to the objective function, and continuously replace the solution vector to obtain a better solution. Finally, the optimal solution of the current iteration is compared with the one before the iteration, and the position information of the optimal solution and the adaptation value is updated.

3) Entering the iterative process, the inertia weight function with nonlinear decay is introduced in the first and middle stages of the iteration to improve the convergence speed, and the elite replacement strategy is introduced in the middle and late stages of the iteration to prevent falling into the local optimal solution.

4) When the calculation reaches the set maximum number of iterations, the Pareto optimal frontier is output and the optimal solution is obtained.

4. Analysis of examples

In this paper, the proposed optimization model for voltage autonomous reactive power control of LV stations containing distributed PV is denoted as Dist-S. In order to validate the effectiveness and feasibility of the proposed algorithm, the effectiveness of the algorithm is verified through the following case studies.

In all the case studies, the node voltage magnitude and line active power obtained from local measurements will be used to update the original and dyadic variables. The maximum operating deviation of the node voltage magnitude is ±0.5 p.u. All the simulation calculations are carried out on MATLAB 2020a on a personal computer with a system hardware environment of Intel Core i7-8265U CPU @ 1.60GHz, 8.00 GB of RAM, and an operating system of win10 64bit.

In this paper, the IEEE 123 node system is used as an example of three-phase asymmetrical operation distribution network arithmetic, which has a voltage level of 0.41 kV. Voltage magnitudes in the case study are expressed as unit values. Each PV system has a generating capacity of 200 kW and a rated apparent power of 1.05 × 200 kVA.

4.1. Comparison of control strategy performance

The performance of the proposed Dist-S is compared with four other benchmark methods.

The first benchmark method is Q(V) sag control, denoted as Droop.

The second is a distributed online reactive power control method based on the ADMM algorithm, denoted as D-ADMM, whose objective is to reduce the voltage deviation.

The third and fourth methods are all centralized control methods, i.e., Cen-linear and Cen-SDP.It is worthwhile to note that the standard form of voltage-reactive power control curves are used here, and hence there is no need to optimize their parameters.

To speed up the convergence of the Dist-S algorithm, the step size is scaled diagonally. $\overline{\gamma}_i$ and $\underline{\gamma}_i$ are chosen to be $0.9/B_{ii}$, where B_{ii} is the diagonal element in the ith row of the matrix B.

For a comprehensive comparison, two representative static scenarios are considered, viz:

1) Scenario 1: It often occurs at noon when the PV is at peak generation, 95% of the peak capacity and the load demand is at 60% of the peak load, the PV is generating excess power thus leading to overvoltage.

2) Scenario 2: Often occurs at night when the PV is not available and the load demand is at its peak, resulting in undervoltage.

The network loss comparison between the proposed method in this paper and other control methods is shown in Table 1. In the IEEE 123-node system case study half-positive definite relaxation is inaccurate. Therefore, the network loss derived by the Cen-SDP method only represents the lower bound of the global optimum. It is worthwhile to note that the network losses in the table are obtained from the trend calculations using the forward back generation again after the successful suppression of voltage crossings by each method.

From the table, it can be seen that the network loss of the Cen-SDP method is the lowest in both scenarios, but the optimal value obtained by it is the lower bound of the minimum network loss, so it is used as a benchmark reference. The network loss produced by the Dis-S method proposed in this paper is only slightly higher than 1.1% of the lower bound of the global minimum network loss value. Therefore, it is verified that the proposed Dis-S method is close to the global optimality. It should be noted that even though the Cen-SDP method produces the minimum network loss, it is also difficult to generalize to real-time voltage control due to its considerable computational and communication burden. In addition, the network losses of the Cen-linear method in Scenario 1 are higher than those of the proposed Dis-S method. This difference is due to the mismatch of the tidal model and the approximation error of the node voltages.

Table 1. The comparison of the method and other control methods in this paper

Method	Scenario 1		Scenario 2	
	Net loss(kW)	Ratio	Net loss(kW)	Ratio
Dist-S	421.6	1.0110	72.4	1.0028
Droop	480.0	1.1511	82.3	1.1399
D-ADMM	479.3	1.1494	89.0	1.2327
Cen-linear	459.2	1.1012	72.7	1.0069
Cen-SDP	417.0	1.000	72.2	1.000

The three-phase voltage distributions of different methods for Scenario 1 are shown in Fig. 3.The voltage distributions using the Cen-linear method in Scenario 1 are slightly different from those of the Dist-S method proposed in this paper.

The upper voltage limit is 1.06, and only the three-phase voltage distributions of Va, Vb, and Vc of the Dist-S method proposed in this paper are within the voltage limit.The three-phase voltage distributions produced by the Cen-SDP method are beyond the upper voltage limit, and are distributed in the range of [1.02,1.08].

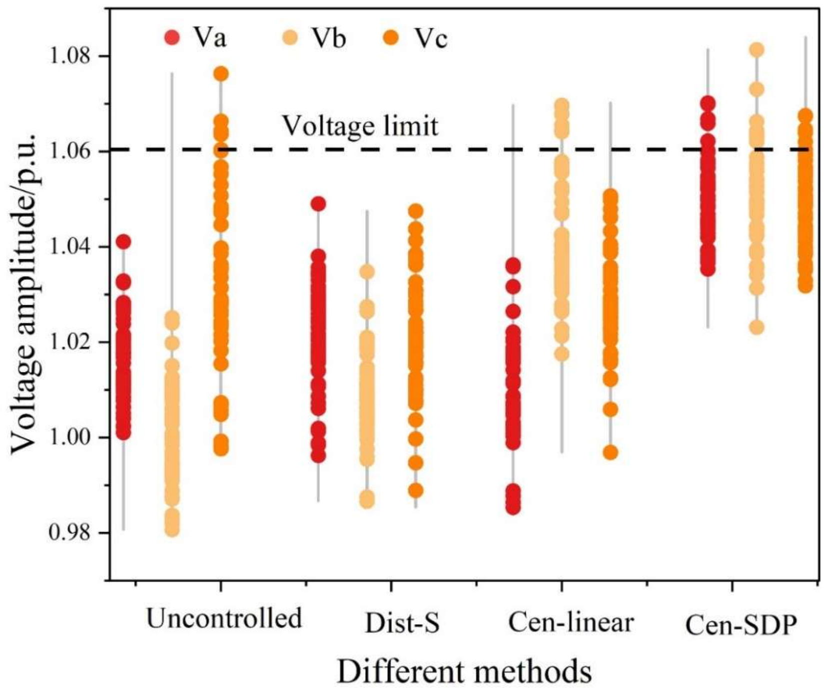

Fig. 3. Scenario 1 the three-phase voltage distribution of different methods

The three-phase voltage distribution for different methods in scenario 2 is shown in Fig. 4. The voltage distributions using the Cen-linear and Dist-S methods in scenario 2 are very similar. It should be noted that the voltage distribution is very different from the other two methods due to the imprecise relaxation of the rank constraint in the Cen-SDP method.The Dist-S method produces a more centralized three-phase voltage distribution, with the three-phase voltage data stably distributed in the range [0.96,1.02].

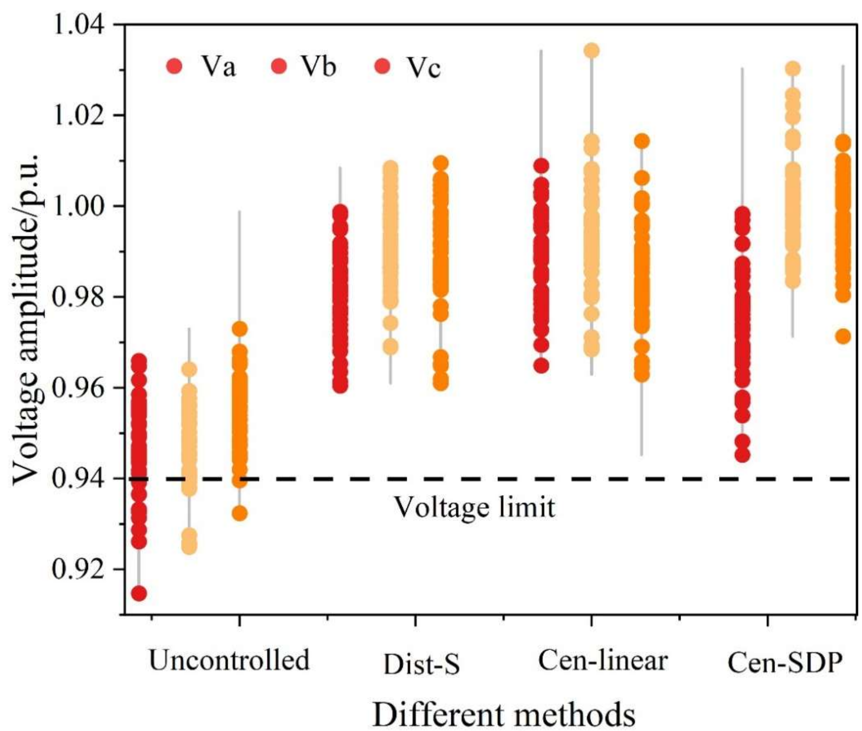

Fig. 4. Scenario 2 the three-phase voltage distribution of different methods

4.2. Robustness analysis of the proposed approach

In order to verify the communication robustness of the proposed optimization method for voltage autonomous reactive power control of LV stations containing distributed PV, a communication packet loss scenario study is carried out. Packet loss occurs between any two neighboring subjects with a packet loss rate of ρ. If the PV system is unable to receive information from a neighboring system within a certain period of time, the information obtained in the last iteration is used.

The voltage magnitude and network loss after 20 iterations under scenario 1 are shown in Table 2. The scenario when ρ is 0 indicates perfect communication and is used as a benchmark. 1000 simulations are performed separately for scenarios with different packet loss rates. The maximum voltage amplitude/p.u (standard deviation) ranges from [1.057,1.057(8.50e-5)] when ρ takes the value of 0-0.5.

Table 2. The post-iteration voltage amplitude and network loss in scenario 1

Probability	Maximum voltage amplitude/p.u(standard deviation)	Network loss/KWW (standard deviation)
0	1.057(0)	432.511(0)
0.1	1.057(4.5939e-5)	431.021(0.0559)
0.2	1.057(6.1124e-5)	431.002(0.0632)
0.3	1.057(6.8056e-5)	431.685(0.0728)
0.4	1.057(7.11e-5)	431.947(0.08082)
0.5	1.057(8.50e-5)	431.996(0.09321)

The voltage magnitude and network loss after 20 iterations under scenario 2 are shown in Table 3. When ρ is 0, the minimum voltage magnitude/p.u (standard deviation) and network loss/KW (standard deviation) are 0.964(0)p.u and 67.239(0)KW, respectively.

Combined with the maximum voltage magnitude and network loss values under 20 iterations under scenario 1, it can be seen that the network loss and voltage magnitude under the voltage autonomous reactive power control optimization method for LV stations containing distributed PV vary very little with the increase in the communication loss rate. Since the Dist-S method proposed in this paper requires the measurement of the system operating state at the beginning of each iteration, the changes in the system conditions can be captured. Even if the system conditions change abruptly during the neighboring iteration period, the last information is reused after data packet loss. However, due to the short iteration interval, the response can be quickly tracked in a new iteration. Therefore, the reuse of the last information after packet loss has less impact on the control algorithm. Therefore, the Dist-S method proposed in this paper is robust to communication faults.

Table 3. The post-iteration voltage amplitude and network loss of 20 iterations

Probability	Maximum voltage amplitude/p.u(standard deviation)	Network loss/KWW (standard deviation)
0	0.964(0)	67.239(0)
0.1	0.963(6.235e-5)	67.332(0.0251)
0.2	0.963(7.782e-5)	67.583(0.02793)
0.3	0.963(8.569e-5)	67.754(0.28904)
0.4	0.963(9.213e-5)	67.893(0.32014)
0.5	0.963(0.975e-5)	67.908(0.35035)

4.3. Comparison of node voltage before and after control

The following are the comparison statistics of node voltage before and after energy storage control and node voltage offset at different seasons 12 respectively, node 23 is the point of minimum value of node voltage offset at that moment and node 45 is the point of maximum value of node voltage offset. From the following four tables, it can be seen that the optimization strategy proposed in this paper for voltage autonomous reactive power control of LV station area containing distributed PV has good effect on all the nodes that cross the limit.

1) Spring. The before and after comparison of load node control in spring is shown in Table 4. The node voltage values are all reduced under the optimization strategy of voltage autonomous reactive power control for LV stations containing distributed PV, and the voltage excursion is controlled within the range of 2.66% to 4.10%.

Table 4. The spring load node control is compared

Node number	Precontrol		After control	
	Node voltage/kv	Voltage offset / %	Node voltage/kv	Voltage offset / %
Node 6	0.5035	22.80	0.4236	3.32
Node 15	0.5017	22.37	0.4213	2.76
Node 20	0.5023	22.51	0.4245	3.54
Node 23	0.5008	22.15	0.4209	2.66
Node 45	0.5057	23.34	0.4268	4.10

2) Summer. Comparison before and after control of load nodes in summer is shown in Table 5. After the adjustment of voltage autonomous reactive power control optimization strategy for LV stations containing distributed PV, the maximum voltage offset of the load node in summer is 3.76%.

Table 5. The summer load node control is compared

Node number	Precontrol		After control	
	Node voltage/kv	Voltage offset / %	Node voltage/kv	Voltage offset / %
Node 6	0.5035	22.80	0.4216	2.83
Node 15	0.5011	22.22	0.4203	2.51
Node 20	0.5009	22.17	0.4235	3.29
Node 23	0.5005	22.07	0.4204	2.54
Node 45	0.5046	23.07	0.4254	3.76

3) Fall. The comparison before and after control of load nodes in fall is shown in Table 6. The maximum value of voltage offset in autumn before control is 23.95%, and the node voltage offset in autumn can be reduced by up to 21.22% after control by the optimization strategy proposed in this paper, which reduces the node voltage offset significantly and optimizes the overall load carrying capacity of the distributed PV distribution network.

Table 6. The fall load node control is compared

Node number	Precontrol		After control	
	Node voltage/kv	Voltage offset / %	Node voltage/kv	Voltage offset / %
Node 6	0.5075	23.78	0.4233	3.24
Node 15	0.5025	22.56	0.4215	2.80
Node 20	0.5017	22.37	0.4246	3.56
Node 23	0.5009	22.17	0.4212	2.73
Node 45	0.5082	23.95	0.4277	4.32

4) Winter. The comparison before and after control of load nodes in winter is shown in Table 7. Before and after the optimization strategy control, the voltage values of node 6, node 15 and node 48 are reduced by 0.083, 0.0802 and 0.0808, respectively.

Table 7. The winter load node control is compared

Node number	Precontrol		After control	
	Node voltage/kv	Voltage offset / %	Node voltage/kv	Voltage offset / %
Node 6	0.5087	24.07	0.4257	3.83
Node 15	0.5036	22.83	0.4234	3.27
Node 20	0.5025	22.56	0.4252	3.71
Node 23	0.5014	22.29	0.4217	2.85
Node 45	0.5090	24.15	0.4282	4.44

4.4. Objective function values before and after control

Comparison of the objective function values before and after the optimization strategy control is shown in Table 8, where representative time nodes of different seasons are selected. After the optimization strategy control, the branch circuit active losses remain within 0-8kW on March 25-26 and December 25-26, respectively. Compared with before the implementation of the optimization strategy, the branch circuit active losses are reduced by 25.9kW and 25.076kW on March 25 and 26, respectively.

It can be seen that adopting the optimization strategy of voltage autonomous reactive power control in LV area with distributed PV proposed in this paper has a practical effect on suppressing the voltage overruns at LV distribution network nodes and reducing the branch circuit active losses in the distribution network.

Table 8. Compare the target function value of the optimal strategy control

Time	Precontrol			After control		
	Voltage shift	Energy storage battery exchange power/kW	The work loss of the branch road/kW	Voltage shift	Energy storage battery exchange power/kW	The work loss of the branch road/kW
3/25	40.513	-	17.596	32.963	785.06	7.063
3/26	39.795	-	17.023	32.214	767.21	7.138
6/25	38.662	-	16.559	33.296	559.34	6.232
6/26	37.780	-	16.427	34.089	561.25	5.965
9/25	41.206	-	17.889	34.158	695.32	5.543
9/26	40.783	-	17.936	34.692	689.69	5.896
12/25	38.664	-	19.253	31.269	721.34	7.235
12/26	37.521	-	20.627	30.095	745.08	7.362

4.5. Comparison of branch circuit active losses

The branch circuit active power loss comparison is shown in Fig. 5. The figure shows the comparison of the active power loss of the branch circuit of the distributed PV LV distribution network before and after the control is taken to access different proportions of distributed PV. The circle indicates the branch circuit active power loss of LV distribution network before control, and the sphere indicates the branch circuit active power loss of LV distribution network after control.

When the proportion of PV is 40%, the node voltage of the low-voltage distribution network is in the critical state of node voltage overrun, and the voltage control strategy proposed in this paper is adopted, and the branch circuit active power loss rises slightly.

When with the further increase of distributed PV access proportion, after taking the low voltage area voltage autonomous reactive power control optimization strategy, the branch circuit active power loss has a significant downward trend. When the proportion of distributed PV is 100%, according to the results of the trend calculation, the branch circuit active power loss of the LV distribution network is reduced by up to 60%.

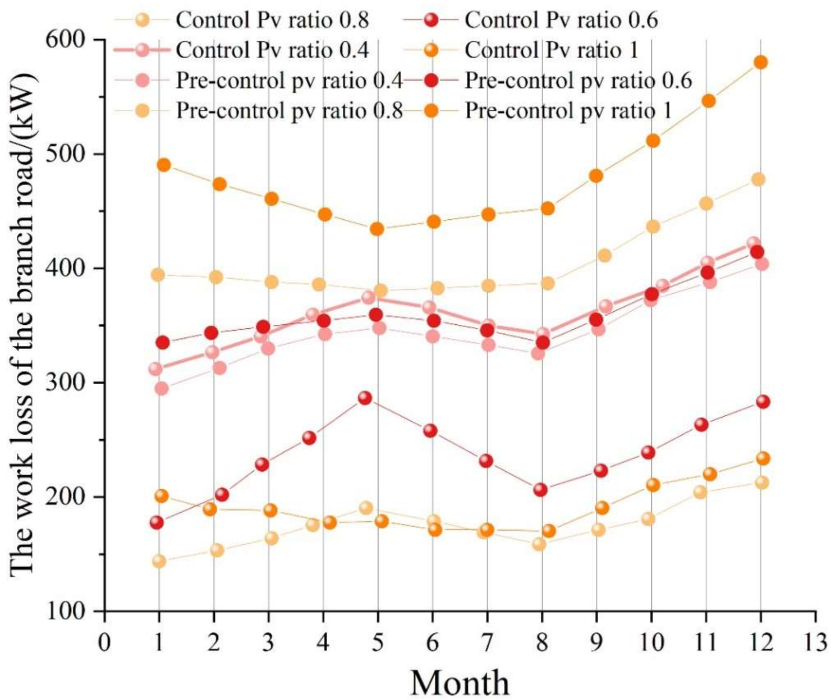

Fig. 5. The support is compared to the loss

5. Conclusion

In this paper, the low-voltage distributed photovoltaic (PV) distribution substations set up in this paper follow the principle of regional autonomy, integrate the terminal edge computing function and the intra-group autonomy strategy, and propose the optimization strategy of voltage autonomous reactive power control for low-voltage substations to realize voltage quality improvement and active loss reduction. The improved MPA algorithm is used to solve the voltage autonomous reactive power optimization control model.

1) The IEEE 123-node system is used as an example of a three-phase asymmetrical operation distribution network, and the three-phase voltages Va, Vb, and Vc generated by the Cen-SDP method in static scenario 1 exceed the upper voltage limit. The voltage distribution of the Cen-linear method in static scenario 2 is similar to that of the Dist-S method in this paper, but the voltage distribution of the Dist-S method in this paper is more centralized. In both classical static scenarios, taking the network loss of Cen-SDP method as a benchmark reference, the network loss of Dist-S method in this paper is lower compared with other models.The network loss and voltage magnitude under the control of Dist-S method change very little with the increase of communication loss rate, so that it can be said that the methodology strategy proposed in this paper is more capable of reducing the network loss and lowering the voltage magnitude.

2) The node voltages and node voltage offsets after control in different seasons are significantly reduced compared to the pre-control period, and the optimization strategy for autonomous reactive power control of LV district voltage with distributed PV has good results for all the nodes that cross the limits.

Under the optimization strategy of autonomous reactive power control of LV district voltage, the branch circuit active power loss decreases with the increase of the proportion of distributed PV access. When the proportion of distributed PV is 100%, the branch circuit active power loss of LV distribution network is reduced by up to 60%.

References

[1] Charfi, W., Chaabane, M., Mhiri, H., & Bournot, P. (2018). Performance evaluation of a solar photovoltaic system. Energy Reports, 4, 400-406.

[2] Hussin, F., Issabayeva, G., & Aroua, M. K. (2018). Solar photovoltaic applications: opportunities and challenges. Reviews in Chemical Engineering, 34(4), 503-528.

[3] Gorjian, S., Zadeh, B. N., Eltrop, L., Shamshiri, R. R., & Amanlou, Y. (2019). Solar photovoltaic power generation in Iran: Development, policies, and barriers. Renewable and Sustainable Energy Reviews, 106, 110-123.

[4] El Hammoumi, A., Chtita, S., Motahhir, S., & El Ghzizal, A. (2022). Solar PV energy: From material to use, and the most commonly used techniques to maximize the power output of PV systems: A focus on solar trackers and floating solar panels. Energy Reports, 8, 11992-12010.

[5] Xuan, Z., Gao, X., Li, K., Wang, F., Ge, X., & Hou, Y. (2020). PV-load decoupling based demand response baseline load estimation approach for residential customer with distributed PV system. IEEE Transactions on Industry Applications, 56(6), 6128-6137.

[6] Garlet, T. B., Ribeiro, J. L. D., de Souza Savian, F., & Siluk, J. C. M. (2019). Paths and barriers to the diffusion of distributed generation of photovoltaic energy in southern Brazil. Renewable and Sustainable Energy Reviews, 111, 157-169.

[7] Xin-gang, Z., & Zhen, W. (2019). Technology, cost, economic performance of distributed photovoltaic industry in China. Renewable and Sustainable Energy Reviews, 110, 53-64.

[8] Wang, L., Yuan, M., Zhang, F., Wang, X., Dai, L., & Zhao, F. (2019). Risk assessment of distribution networks integrating large-scale distributed photovoltaics. IEEE access, 7, 59653-59664.

[9] Yu, S., Han, R., & Zhang, J. (2023). Reassessment of the potential for centralized and distributed photovoltaic power generation in China: On a prefecture-level city scale. Energy, 262, 125436.

[10] Rahdan, P., Zeyen, E., Gallego-Castillo, C., & Victoria, M. (2024). Distributed photovoltaics provides key benefits for a highly renewable European energy system. Applied Energy, 360, 122721.

[11] da Silva, P. P., Dantas, G., Pereira, G. I., Câmara, L., & De Castro, N. J. (2019). Photovoltaic distributed generation–An international review on diffusion, support policies, and electricity sector regulatory adaptation. Renewable and sustainable energy reviews, 103, 30-39.

[12] Gui, Y., Nainar, K., Bendtsen, J. D., Diewald, N., Iov, F., Yang, Y., ... & Stoustrup, J. (2023). Voltage support with PV inverters in low-voltage distribution networks: An overview. IEEE Journal of Emerging and Selected Topics in Power Electronics, 12(2), 1503-1522.

[13] Ruan, H., Gao, H., Liu, Y., Wang, L., & Liu, J. (2020). Distributed voltage control in active distribution network considering renewable energy: A novel network partitioning method. IEEE Transactions on Power Systems, 35(6), 4220-4231.

[14] Stringer, N., Haghdadi, N., Bruce, A., Riesz, J., & MacGill, I. (2020). Observed behavior of distributed photovoltaic systems during major voltage disturbances and implications for power system security. Applied Energy, 260, 114283.

[15] Li, R., Wong, P., Wang, K., Li, B., & Yuan, F. (2020). Power quality enhancement and engineering application with high permeability distributed photovoltaic access to low-voltage distribution networks in Australia. Protection and Control of Modern Power Systems, 5(3), 1-7.

[16] Yili Ma,Yi Huang & Yue Yuan. (2025). The short-term forecasting of distributed photovoltaic power considering the sensitivity of meteorological data. Journal of Cleaner Production,486,144599-144599.

[17] Yubo Wang,Chao Huo,Fei Xu,Libin Zheng & Ling Hao. (2025). Ultra-Short-Term Distributed Photovoltaic Power Probabilistic Forecasting Method Based on Federated Learning and Joint Probability Distribution Modeling. Energies,18(1),197-197.

[18] Emmanuel Philibus,Azlan Mohd Zain,Didik Dwi Prasetya,Mahadi Bahari,Norfadzlan bin Yusup,Rozita Abdul Jalil... & Azurah A Samah. (2025). Marine Predator Algorithm and Related Variants: A Systematic Review. International Journal of Advanced Computer Science and Applications (IJACSA),16(1).

[19] Yang Shen,Deyi Li,Wenbo Wang & Xu Dong. (2024). Blood Glucose Concentration Prediction Based on Double Decomposition and Deep Extreme Learning Machine Optimized by Nonlinear Marine Predator Algorithm. Mathematics,12(23),3708-3708.